Measurement of cross-sectional velocity distribution of pneumatically conveyed particles in a square-shaped pipe through electrostatic sensing and Gaussian process regression

Yongyue Wang
School of Control and Computer Engineering
North China Electric Power University
Beijing, China
y.wang@ncepu.edu.cn

Lijuan Wang
School of Engineering
University of Kent
Canterbury, Kent, U. K.
l.wang@kent.ac.uk

Xiangchen Qian
School of Control and Computer Engineering
North China Electric Power University
Beijing, China
xqian@ncepu.edu.cn

Yong Yan
School of Engineering
University of Kent
Canterbury, Kent, U. K.
y.yan@kent.ac.uk

***Abstract*—Online continuous measurement of the cross-sectional velocity distribution of pneumatically conveyed solids in a square-shaped pipe is desirable in monitoring and optimizing circulating fluidized beds, coal-fired power plants and exhaust pipes. Due to the limitation of non-invasive electrostatic sensors in spatial sensitivity, it is difficult to accurately measure the velocity of particles in large diameter pipes. In this paper, a novel approach is presented for the measurement of cross-sectional particle velocity distribution in a square-shaped pipe using sensors and Gaussian process regression (GPR). The electrostatic sensor includes twelve pairs of strip-shaped electrodes. Experimental tests were conducted on a laboratory test rig to measure the cross-sectional particle velocities in a vertical square pipe under various experimental conditions. The GPR model is developed to infer the relationship between the input variables of velocities and the cross-sectional velocity distribution of particles. Results obtained suggest that the electrostatic sensor in conjunction with the GPR model is a feasible approach to obtain the cross-sectional velocity distribution of pneumatically conveyed particles in a square-shaped pipe.**

Keywords—two-phase flow, particle velocity, Gaussian process regression, square-shaped pipe, cross-sectional velocity distribution.

I. INTRODUCTION

Square-shaped pneumatic conveying pipes are commonly used in circulating fluidized beds, coal-fired power plants in certain countries, e.g., Poland and Germany [1], [2]. During the conveying processes, particles are irregularly distributed in the pipe cross section due to the time-varying interphase forces, the variation of pipe direction, properties of the particles and phase loading ratio. Therefore, cross-sectional velocity measurement of particles in gas–solid two-phase flows in square-shaped pipes is of great significance to understanding the dynamic behaviors of particles and the determination of the mass flow rate of solids. However, there is little research on the cross-sectional characterization of gas–solid two-phase flow in square-shaped pipes.

The radiometric, optical and microwave sensors can be used to measure the cross-sectional velocity distribution of particles [3], [4]. However, they are not suitable for industrial measurement due to the high cost and susceptibility to interference from harsh industrial environments. Compared with these sensors, electrostatic sensors have the advantages of simple structure, cost-effectiveness and suitability for a wide range of installation conditions [5]. Electrostatic sensors are based on the principle of electrostatic induction. The electrode in an electrostatic sensor is insulated and screened from external electromagnetic interference. A signal conditioning circuit is used to amplify and filter the weak signal from the electrode [2], [6]. In most practical pneumatic conveying processes fluctuations in the temperature and pressure of the conveying air have little impact on the performance of the electrostatic sensors. However, changes in the dielectric properties and physical quantities (e.g. velocity) of pneumatically conveyed particles affect the amplitude and frequency charateristics of the sensor signal [7].

Particularly, non-invasive electrostatic sensors are more suitable for industrial applications because they exhibit a significant advantage in their non-restrictiveness to the movement of particles in a pipe. However, due to the fast weakening sensitivity with the increasing distance from the sensing electrode to moving particles, the use of non-invasive electrostatic sensors in a ring shape, arc shape or strip shape on circular pipelines demonstrate uncertain accuracy in the measurement of cross-sectional averaged velocity in large pipes under different flow conditions [5]. Due to the non-circle center symmetry and the existence of four right angles on the pipe wall, particle distribution in a square-shaped pipe is more complex than that in a circular-shaped pipe. Therefore, the limitations of traditional measurement methods need to be addressed urgently.

In recent years, soft computing techniques have been widely applied to facilitate the characterization of multiphase flow by establishing the relationship with the variables that can be measured directly [8]. For example, convolutional neural networks were developed for patterns identification of multiphase flows [9], [10], [11]. Artificial neural network (ANN) and support vector machine (SVM) were trained with experimental data to measure the mass flow rate and the fraction of individual phase in gas–solid or gas–liquid two-phase flows [12], [13], [14], [15]. There is also research combining electrical capacitance tomography (ECT) techniques with deep-learning algorithms to visualize the dynamics of gas–liquid two-phase flow [16], [17]. While the study applies soft computing techniques to cross-sectional velocity distribution measurement of particles in gas–solid two-phase flows is rare. However, with its wide application

and superior performance in multiphase flow measurement, soft computing provides a new idea for the measurement of cross-sectional particle velocity distribution.

Gaussian process regression (GPR) has been gradually recognized as a useful soft sensor modeling method over the past few years due to its excellent performance [18], [19]. Compared with common machine learning algorithms including SVM, ANN and regression trees, GPR has good adaptability and strong generalization ability to deal with complex problems such as high dimensions, small samples and nonlinearity. This paper presents a novel approach incorporating electrostatic sensing with Gaussian process regression (GPR) modeling for the measurement of cross-sectional velocity distribution of pneumatically conveyed particles in a square-shaped pipe. The particle velocities measured by twelve pairs of non-invasive electrodes and the air velocity are used as the input variables of the model, while the output variables of the model are particle velocities in different areas of the pipe cross section. Evaluation tests were undertaken to verify the performance of the proposed measurement approach.

II. Methodology

A. Overall Measurement Strategy

The overall strategy for the measurement of the cross-sectional velocity distribution of particles in a square-shaped pipe is shown in Fig. 1. The non-invasive electrostatic sensor that consists of twelve pairs of strip-shaped electrodes is used to measure the velocity of particles moving through each electrode pair. Two identical parallel electrodes, one being positioned downstream of the other, are used to determine particle velocity using a cross-correlation technique [5]. The air velocity is obtained with a measuring device suitable for the flow conditions. Then the twelve particle velocities and the air velocity are considered as input variables to the model. In order to reduce the dimensionality of datasets and increase interpretability, principal component analysis (PCA) is applied to the input variables. The vectors (i.e. principal components) from PCA are fed into the GPR model. Then the cross-sectional velocity distribution of particles in a square-shaped pipe is obtained by the GPR model.

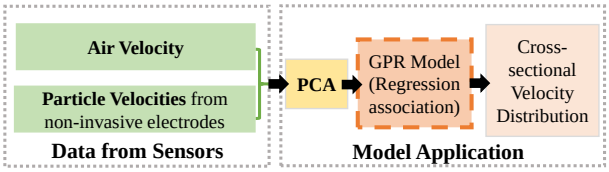

Fig. 1. Principle of the measurement strategy.

B. Sensors

The structure of the sensor used in this study is shown in Fig. 2. The non-invasive electrostatic sensor consists of twelve pairs of strip-shaped electrodes (three pairs on each inner surface of the pipe). All the stripe-shaped copper electrodes have the same dimension with a length of 15 mm and a width of 3 mm [2]. The holes on the pipe wall are used to insert a device for the measurement of pure air velocity. In order to simultaneously obtain the reference velocities of particles in different areas of the pipe cross section, an invasive electrostatic sensor including nine pairs of electrodes with the same dimensions of the non-invasive electrodes is installed downstream from the holes. The distance between the non-invasive electrostatic sensor and the invasive electrostatic sensor is 16 cm which is enough to avoid the turbulence caused by the invasive electrostatic sensor. The sensor is covered in a grounded shielding case to isolate both sensor arrays from external electromagnetic interference [2]. As shown in Fig. 3, the pipe cross section with the side length of 54 mm is equally divided into nine sub-areas (index by A1-A9) and each invasive electrode is placed in the area center. Therefore, the reference particle velocities of each area of the square pipe can be obtained by nine pairs of electrodes, respectively. Then the reference particle velocities are used as the output variables in the model training process.

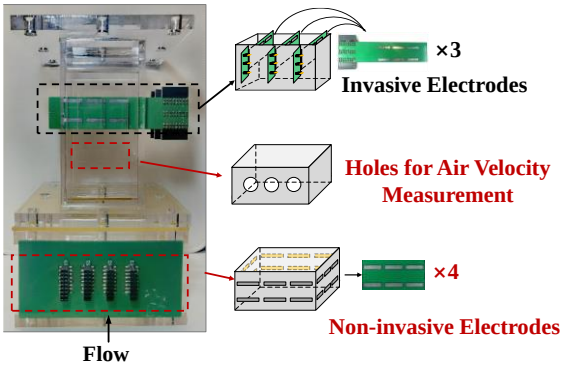

Fig. 2. Structure of non-invasive and invasive electrostatic sensors.

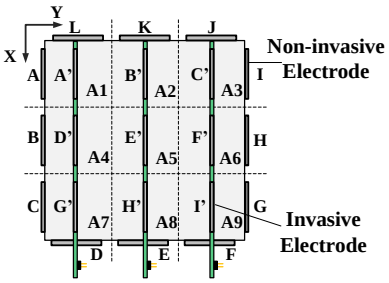

Fig. 3. Division of square-shaped pipe cross section and electrode configuration.

C. Principal Component Analysis

The input variables include twelve particle velocities (namely v_A to v_L) which are obtained from twelve pairs of non-invasive electrodes and the air velocity (v). It is found that the input variables are correlated with each other to some extent. Therefore, PCA is used to remove the redundancy information and reduce the dimensionality of the predictor space, which can help prevent overfitting in the model training process. PCA is used to linearly transform the predictive factors, remove redundant dimensions, and generate a group of new variables called principal components. Firstly, the potential input variables are normalized as a matrix $X_{m\times n}$ and the covariance matrix C is calculated by:

$$C = \frac{1}{m} X X^T \tag{1}$$

where m is the dimension of X. X^T is the transposed matrix of X. Then the eigenvalues λ and eigenvectors α of the matrix C can be determined by:

$$C\alpha = \lambda\alpha \tag{2}$$

The eigenvalues and corresponding eigenvectors are sorted by $\lambda_1 \geq \lambda_2 \geq \cdots \geq \lambda_n$. The eigenvalues are arranged into a matrix from top to bottom according to the corresponding eigenvectors, and the first k rows are taken to form a matrix M.

$$P = MX \tag{3}$$

where $P = \{p_1, p_2 \cdots p_k\}$ is the set of principal components, k is the reduced dimension. The resulting principal components are uncorrelated and arranged in a descending order according to their significance contributing to the overall data variation. The contribution of P is defined as:

$$\alpha_k = \frac{\sum_{i=1}^{k} \lambda_i}{\sum_{i=1}^{n} \lambda_k} (k \leq n) \quad (4)$$

In this study, PCA keeps enough components to explain 95% variance.

D. Gaussian Process Regression

The difference between the GPR algorithm and general machine learning algorithms such as regression trees, SVM and ANN is that there is a covariance matrix reflecting the correlation between the features of the sample in the Gaussian process, which makes GPR show super fitting ability and more explainable [20]. Therefore, GPR is chosen to describe priority knowledge of processes in this study.

GPR is a non-parametric kernel-based probabilistic model that uses Gaussian process priors to perform regression analysis on data which has advantages over parameterized methods in regression analysis with a limited number of training samples. GPR model is represented as

$$y = h(x)^T \beta + f(x) \quad (5)$$

where $f(x)$ is from a zero-mean Gaussian process with covariance function. In this study, x is the principal components diverted from PCA, the output variables y are particle velocities in different areas of the pipe cross section, $h(x)$ represents a set of functions that transform the original vector x in R^d into a new feature vector $h(x)$ in R^p. d represents the dimension of the original vector. p represents the dimension of the transformed vector, which is consistent with the dimension of $f(x)$. β is a p-by-1 vector of basis function coefficients. The distribution of y_i in the probability model is

$$P(y_i|f(x_i), x_i) \sim N(y_i|h(x_i)^T \beta + f(x_i), \sigma^2) \quad (6)$$

where σ^2 is the error variance of normal distribution data, x_i is the observation of the latent variable $f(x_i)$. In vector form, this model is equivalent to

$$P(y|f, X) \sim N(y|H\beta + f, \sigma^2 I) \quad (7)$$

where

$$X = \begin{pmatrix} x_1^T \\ x_2^T \\ \vdots \\ x_n^T \end{pmatrix}, y = \begin{pmatrix} y_1 \\ y_2 \\ \vdots \\ y_n \end{pmatrix}, H = \begin{pmatrix} h(x_1^T) \\ h(x_2^T) \\ \vdots \\ h(x_n^T) \end{pmatrix}, f = \begin{pmatrix} f(x_1) \\ f(x_2) \\ \vdots \\ f(x_n) \end{pmatrix}.$$

The joint distribution of latent variables $f(x_1), f(x_2) \ldots f(x_n)$ follows:

$$P(f|X) \sim N(f|0, K(X, X)) \quad (8)$$

where $K(X, X)$ is

$$K(X, X) = \begin{pmatrix} k(x_1, x_1) & K(x_1, x_2) & \cdots & k(x_1, x_n) \\ k(x_2, x_1) & k(x_2, x_2) & \cdots & k(x_2, x_n) \\ \vdots & \vdots & \vdots & \vdots \\ k(x_n, x_1) & k(x_n, x_2) & \cdots & k(x_n, x_n) \end{pmatrix} \quad (9)$$

The kernel function $k(x_i, x_y)$ in the Gaussian process regression model reflects the similarity and correlation between different sample sets and plays a key role in the prediction performance of the GPR model. There are four possible kernel functions: the squared exponential kernel (SEK), exponential kernel (EK), Matern 5/2 (M52K) and rational quadratic kernel (RQK). Their functions are defined as

$$k_{SEK}(x_i, x_y) = \sigma_f^2 \exp(-\frac{r^2}{2\sigma_l{}^2}), \quad (10)$$

$$k_{EK}(x_i, x_y) = \sigma_f^2 \exp(-\frac{r}{\sigma_l}), \quad (11)$$

$$k_{M52K}(x_i, x_y) = \sigma_f^2 (1 + \frac{\sqrt{5}r}{\sigma_l} + \frac{5r^2}{3\sigma_l{}^2}) \exp(-\frac{\sqrt{5}r}{\sigma_l}), \quad (12)$$

$$k_{RQK}(x_i, x_y) = \sigma_f^2 (1 + \frac{r^2}{2\alpha\sigma_l{}^2})^{-\alpha}, \quad (13)$$

where σ_i is the characteristic length scale, σ_f is the signal standard deviation and

$$r = \sqrt{(x_i - x_j)^T (x_i - x_j)} \quad (14)$$

is the Euclidean distance between x_i and x_j.

The optimal kernel function can be considered by comparing the prediction effect of models based on different kernel functions. In order to assess the performance of the model in terms of accuracy, the root-mean-square error (RMSE) is calculated based on the reference particle velocities and the predicted particle velocities from the model. By comparing RMSE, the performance of the trained models can be comprehensively understood and evaluated. RMSE is defined as:

$$RMSE = \sqrt{\frac{1}{m} \sum_{i=1}^{m} (y_i - \hat{y}_i)^2} \quad (15)$$

where m is the number of test data, y_i is the reference value of the i-th test, $\hat{y}_i$ is the predicted value of the i-th test.

III. Experimental And Results

A. Experimental Setup

As shown in Fig. 4, experimental tests were carried out on a laboratory-scale test rig consisting of a feeding system, a powder recovery, a negative pressure system and electrostatic sensors. Solid particles (plain flour with the size range of 98–124 μm) were fed into the pipe using the double screw feeder and pneumatically conveyed to the solids recycling tank using the negative pressure system, respectively. The mass flow rate of particles and the conveying velocity can be changed by adjusting the double screw feeder and the negative pressure device, respectively. As shown in Fig. 4, the sensors were installed on a vertical pipe about 1200 mm away from the upstream elbow. The non-invasive electrostatic sensor and the invasive electrostatic sensor were used to measure the particle velocities simultaneously. During data acquisition, variables such as the ambient temperature (around 26℃), relative humidity (around 69%) and particle characteristics (i.e. size, type, moisture content, etc.) were all controlled and almost constant.

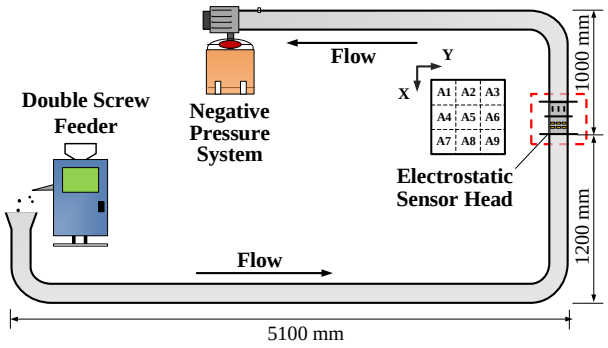

Fig. 4. The layout of the test rig with a square-shaped pipe.

The data used in this study were obtained from 16 experimental conditions (V1M1 to V4M4) as outlined in Table I. The air velocity and mass flow of particles were adjusted from 19 m/s to 31 m/s and 2 kg/h to 8 kg/h, respectively. A total of 4496 datasets were obtained for model training and testing.

TABLE I. EXPERIMENTAL CONDITIONS

Mass Flow (kg/h)	Air velocity (m/s)			
	V1=19	V2=23	V3=27	V4=31
M1=2	V1M1	V2M1	V3M1	V4M1
M2=4	V1M2	V2M2	V3M2	V4M2
M3=6	V1M3	V2M3	V3M3	V4M3
M4=8	V1M4	V2M4	V3M4	V4M4

B. *Kernel Function Selection*

Since the kernel function of the GPR model has an influence on the predicted results, it is necessary to choose a suitable kernel function before model training. In order to evaluate the effects of different kernel functions (EK, M52K, RQK and SEK) on the model performance, four GPR models with different kernel functions were developed based on the same training dataset, respectively. The RMSE results of predicted velocities from four GPR models in areas A1 to A9 are shown in Fig. 5. As can be seen from Fig. 5, the GPR model with the EK kernel function has the lowest RMSE than other models in all areas except for A1 and A6. The difference in RMSE between the GPR model with EK kernel function and the best-performed model is less than 0.5%. Therefore, the exponential kernel function is selected to measure the cross-sectional velocity distribution under experimental conditions.

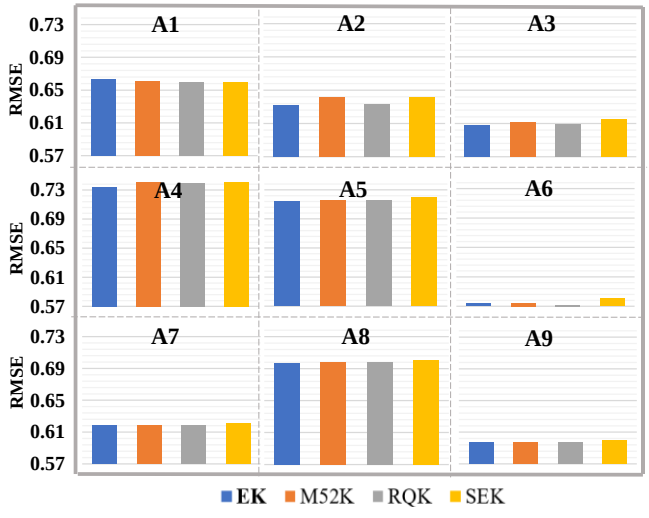

Fig. 5. Comparison of RMSE for four GPR models with different kernel functions.

C. *Experimental Results and Analysis*

In the model training process, the principal component vectors obtained from PCA were taken as the input of the GPR model. The reference particle velocity of each area is regarded as the output variable of the model. The 5-fold cross-validation was applied in the model training process to evaluate the prediction performance of the model, which can also avoid the overfitting of the model. During the model training, the Bayesian optimization was used to optimize the hyperparameter ($\theta = \{\sigma_i,\ \sigma_f,\ \sigma\}$). The algorithm terminates after 30 iterations, because no obvious improvement is observed when the number of iterations is beyond 30. Then the trained model is used to determine the cross-sectional velocity distribution only from the particle velocities measured by the non-invasive electrostatic sensor and the air velocity.

Fig. 6 shows the predicted particle velocities and reference particle velocities of the test dataset in 9 areas under 16 experimental conditions. The predicted velocity values are very close to reference values in all areas. The relative errors between predicted values and the reference values are depicted in Fig. 7. Under all experimental conditions, the relative errors of the predicted velocities in A1 to A9 are all within ±3%. The results suggest that the GPR model is capable of predicting the cross-sectional velocity distribution of particles in a square-shaped pipe based on particle velocities measured by electrostatic sensors along with the velocity of conveying air.

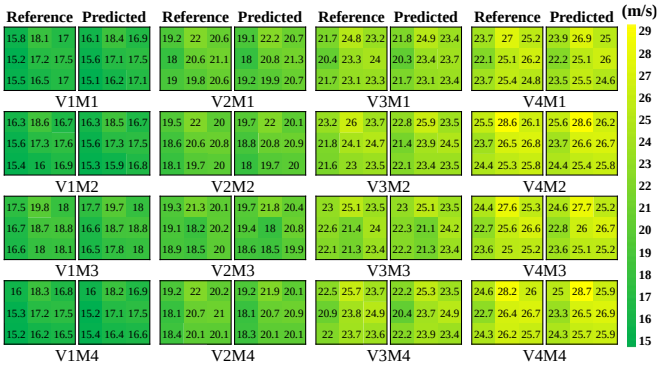

Fig. 6. Comparison of the predicted and reference velocities of the particle under 16 experimental conditions.

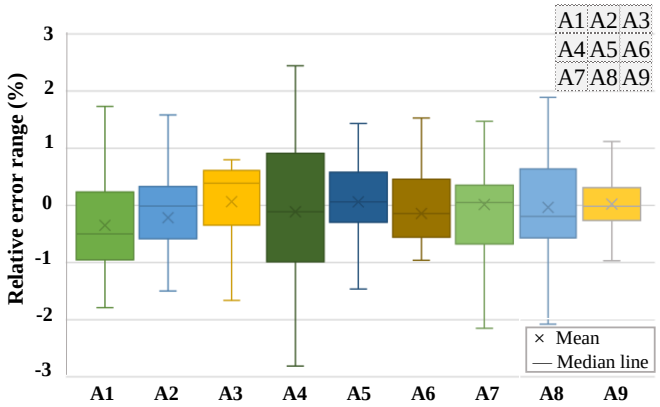

Fig. 7. Relative error range of the predicted velocities in nine areas under all experimental conditions.

The accuracy of the trained model mainly depends on the comprehensiveness of the training data. However, it is

impractical to obtain the training data under all flow conditions. In order to evaluate the performance of the GPR model with a smaller training dataset or missing data, three GPR models that trained using different training datasets were tested with the test datasets shown in Table II, respectively. It is worth noting that the dataset used for training GPR models excludes the flow conditions for testing.

TABLE II. TEST SETUP OF SMALLER TRAINING DATASET

Test group	Test dataset not included in the training dataset
Test I	V1M4, V4M1
Test II	V3M1, V3M2, V3M3, V3M4
Test III	V1M3, V2M3 V3M3 V4M3

In Test I, the GPR model was trained with data from all experimental conditions except for V1M4 (lowest air velocity 19 m/s and highest solid mass flow rate 8 kg/h) and V4M1 (highest air velocity 31 m/s and lowest solid mass flow rate 2 kg/h). The experimental results of these two flow conditions were used to evaluate the trained model. As shown in Fig. 8(a), the relative error of predicted velocity has negative values under the condition of high air velocity and low solid mass flow rate, while the relative error is positive under the condition of low air velocity and high solid mass flow rate. The relative error in all areas is still less than ±5% under the condition of V4M1. However, the relative error of the predicted velocity goes up to the range between 11.60% and 15.16% under the condition of V1M4 because the flow condition is far beyond the training conditions of the model.

In Test II, the training dataset does not contain the data collected at the air velocity of 27 m/s. The developed GPR model was tested under the condition of V3M1, V3M2, V3M3 and V3M4. Fig. 8(b) shows that the relative errors are mostly within ±5% when the solid mass flow rate changes from 2 kg/h to 6 kg/h. When the solid mass flow rate reaches 8 kg/h, larger errors (around 10%) occur in areas A4 and A5. However, compared with the results from Test I, the overall performance is still better than that under the V1M4 flow condition. This is because the test dataset in Test II is unknown to the model but is still within the range of the training dataset.

In Test III, the measurement results under the solid mass flow rate of 6 kg/h were used as the test dataset (not included in the training dataset). The performance of the GPR model under the conditions of V1M3, V2M3, V3M3 and V4M3 is shown in Fig. 8(c). When the air velocity is 19 m/s and 31 m/s, the relative errors in all areas are less than ±3%. But larger errors (around ±8%) occur in areas A4 and A5 when the air velocity is at 23 m/s and 27 m/s. Due to the uneven distribution of data in the training dataset, these flow conditions were mismatched by the model to other flow conditions, which resulted in larger errors. The result also indicates that more features related to flow conditions need to be considered for model training in the follow-up study.

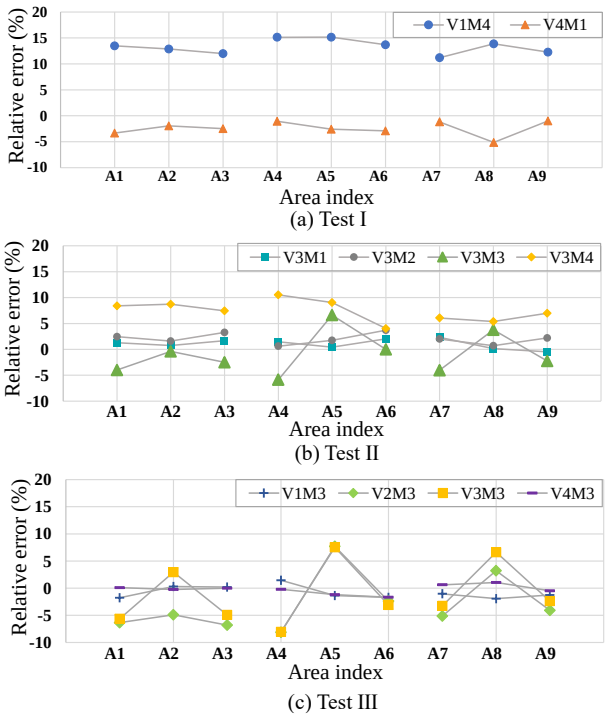

Fig. 8. Relative error for the predicted velocities under different flow conditions.

IV. CONCLUSIONS

In this paper, a novel approach using a non-invasive electrostatic sensor and a GPR model to the measurement of the cross-sectional velocity distribution of pneumatically conveyed particles is proposed and evaluated. The feasibility of the proposed measurement methodology has been verified under laboratory conditions. Experimental results have demonstrated that the GPR model with exponential kernel function trained with the data from all experimental conditions performs well. The relative error of predicted velocities in each area is within 3%. With a smaller training dataset, the model performance is negatively affected. For the data beyond the range of the training dataset, the relative error of the model goes up to ±10% or even ±15%. However, the limitation in generalization ability is a common problem for all data-driven models. In future, investigations into the improvement of the generalization ability of GPR models will be conducted and field trials will be carried out to assess the methodology under industrial conditions.

REFERENCES

[1] B. Jurjevčič, A. Senegačnik, B. Drobnič, and I. Kuštrin, "The Characterization of Pulverized-Coal Pneumatic Transport Using an Array of Intrusive Electrostatic Sensors," IEEE Trans. Instrum. Meas., vol. 64, no. 12, pp. 3434–3443, 2015.

[2] X. Qian, Y. Yan, S. Wu, and S. Zhang, "Measurement of velocity and concentration profiles of pneumatically conveyed particles in a square-shaped pipe using electrostatic sensor arrays," Powder Technol., vol. 377, pp. 693–708, 2021.

[3] Y. Yan, "Mass flow measurement of bulk solids in pneumatic pipelines," Meas. Sci. Technol., vol. 7, no. 12, pp. 1687–1706, 1996.

[4] Y. Zheng and Q. Liu, "Review of techniques for the mass flow rate measurement of pneumatically conveyed solids," Measurement, vol. 44, no. 4, pp. 589–604, 2011.

[5] Y. Yan, Y. Hu, L. Wang, X. Qian, W. Zhang, K. Reda, J. Wu, and G. Zheng, "Electrostatic sensors–Their principles and applications," Measurement, vol. 169, pp. 108506, 2021.

[6] Y. Hu, Y. Yan, X. Qian, and W. Zhang, “A comparative study of induced and transferred charges for mass flow rate measurement of pneumatically conveyed particles,” Powder Technol., vol. 356, pp. 715–725, 2019.

[7] X. Qian, D. Shi, Y. Yan, W. Zhang, and G. Li, “Effects of moisture content on electrostatic sensing based mass flow measurement of pneumatically conveyed particles,” Powder Technol., vol. 311, pp. 579–588, 2017.

[8] Y. Yan, L. Wang, T. Wang, X. Wang, Y. Hu, and Q. Duan, “Application of soft computing techniques to multiphase flow measurement: A review,” Flow Meas. Instrum., vol. 60, pp. 30–43, 2018.

[9] Z. Yang, H. Ji, Z. Huang, B. Wang, and H. Li, “Application of convolution neural network to flow pattern identification of gas-liquid two-phase flow in small-size pipe,” 2017 Chinese Automation Congress (CAC), pp. 1389–1393, 2017.

[10] Z. Xu, F. Wu, L. Zhu, and Y. Li, “LSTM model based on multi-feature extractor to detect flow pattern change characteristics and parameter measurement,” IEEE Sens. J., vol. 21, no. 3, pp. 3713–3721, 2020.

[11] Z. Gao, Z. Qu, Q. Cai, L. Hou, M. Liu and T. Yuan, “A deep branch-aggregation network for recognition of gas–liquid two-phase flow structure,” IEEE Trans. Instrum. Meas., vol. 70, pp. 1–8, 2020.

[12] F. Abbas, Y. Yan, and L. Wang, “Mass flow rate measurement of pneumatically conveyed solids through multimodal sensing and data-driven modeling,” IEEE Trans. Instrum. Meas., vol. 70, pp. 2513416, 2021.

[13] F. Abbas, L.Wang, Y. Yan, “Mass flow rate measurement of solids in a pneumatic conveying pipeline in different orientations,” Measurement: Sensors, vol. 10, pp. 100021, 2020.

[14] L. Wang, J. Liu, Y. Yan, X. Wang, and T. Wang, “Gas-liquid two-phase flow measurement using Coriolis flowmeters incorporating artificial neural network, support vector machine, and genetic programming algorithms,” IEEE Trans. Instrum. Meas., vol. 66, no. 5, pp. 852–868, 2016.

[15] H. Wang, M. Zhang, and Y. Yang, “Machine learning for multiphase flowrate estimation with time series sensing data,” Measurement: Sensors, vol. 10, pp. 100025, 2020.

[16] C. Tan, S. Lv, F. Dong, and M. Takei, “Image reconstruction based on convolutional neural network for electrical resistance tomography” IEEE Sens. J., vol. 19, no. 1, pp. 196–204, 2018.

[17] J. Zheng and L. Peng, “An autoencoder-based image reconstruction for electrical capacitance tomography,” IEEE Sens. J., vol. 18, no. 13, pp. 5464–5474, 2018.

[18] J. Li, Y. Qu, C. Li, Y. Xie, Y. Wu, and J. Fan, “Learning local Gaussian process regression for image super-resolution,” Neurocomputing, vol. 154, pp. 284–295, 2015.

[19] J. Hu, and J. Wang, “Short-term wind speed prediction using empirical wavelet transform and Gaussian process regression,” Energy, vol. 93, pp. 1456–1466, 2015.

[20] .Y. Jiang, J. Jia, Y. Li, Y. Kou, and S. Sun, “Prediction of gas-liquid two-phase choke flow using Gaussian process regression,” Flow Meas. Instrum., vol. 81, pp. 102044, 2021.